Supplement of

Role of Criegee intermediates in the formation of sulfuric acid at a Mediterranean (Cape Corsica) site under influence of biogenic emissions

Alexandre Kukui, et al.

Table of content

S1 Previous studies

Table S1. Previous results on the H_2SO_4 budget based on the studies including OH, H_2SO_4, SO_2 and particles measurements

Air type	Location	SO_2, ppb	Condensation sink (CS), s^{-1}	Used k_{OH+SO2}, cm^3 mlk^{-1} s^{-1} (298K, 1Atm)	Ratio of $[H_2SO_4]$ /[OH]	Ratio of H_2SO_4 production in $OH+SO_2$ /Loss (if uptake = 1)	Ref
Remote continental 3000 m a.s.l.	Idaho Hill, Rocky Mountains, Colorado, TOHPE, September 1993	≈ 0.5 [a)]	6×10^{-3} [b)]	8.5×10^{-13}	1 – 2 [a)]	≈ 1	(Weber et al., 1997)
Remote marine, 3400 m a.s.l.	Mauna Loa Obs., Hawaii July, 1992	≈ 0.5 [a)]	$10^{-3} – 10^{-2}$	8.5×10^{-13}	≈ 1 [a)]	1	(Weber et al., 1997)
Remote marine, polar	Anvers Island, western Antarctica, SCATE, Jan.-Feb., 1994	0.01-0.02	$10^{-4} – 10^{-3}$	8.5×10^{-13}	8.7 [c)]	≈ 0.1	(Jefferson et al., 1998)
Forested rural continental mountain site	Fritz Peak Obs., Colorado, June-August, 1991	0.2-1 [a)]	≈ 5×10^{-3} [a)]	8.5×10^{-13}	≈ 1 [a)]	0.5 - 1	(Eisele and Tanner, 1993)
	Hohenpeissenberg, southern Germany April, 1998	≈ 0.3 [a)]	-	8.5×10^{-13}	≈ 1.5 [a)]	≈ 1 >1 [e)]	(Birmili et al., 2000)
	Hohenpeissenberg, southern Germany HAFEX 2000 April and June, 2000	≈ 0.3 [a)]	≈10^{-2} [a)]	8.06×10^{-13}	≈ 1 [a)]	≈ 1 day <0.5 night	(Boy et al., 2013)
	Hohenpeissenberg, southern Germany HOPE 2012 11/07-19/08, 2012	0.09 [c)]	7×10^{-3} [c)]	1.3×10^{-12}	0.5 [c)]	1.1	(Novelli et al., 2017)
Remote Coastal	Mace Head, Ireland PARFORCE June, 1999	0.1-1 [a)]	$5\times10^{-3} – 10^{-2}$ [a)]	8.5×10^{-13}	≈ 5 [a)]	< 0.03	(Berresheim et al., 2002)
	Mace Head, Ireland 2010-2011	≈ 0.2 [a)]	≈ 3×10^{-3} [a)]	9×10^{-13}	7.1 [c)]	≈ 0.2	(Berresheim et al., 2014)
	Finokalia, northern coast of Crete (Eastern Mediterranean) MINOS, August, 2001	≈ 1 [a)]	≈ 10^{-2} [a)]	8.5×10^{-13}	1 - 5 [a)]	≈ 0.5	(Bardouki et al., 2003)
Boreal Forest	Hyytiälä, Finland EUCAARI March - June, 2007	-	-	8.5×10^{-13}	1.8 [b)]	<0.5	(Petäjä et al., 2009)
	Hyytiälä, Finland HUMPPA-COPEC-2010 Jul. – Aug., 2010	0.6 [d)]	5.5×10^{-3} [b)]	8.5×10^{-13}	2.8 [d)]	≈ 0.4	(Mauldin III et al., 2012)
		0.03-0.3[a)]	≈10^{-2} [a)]	8.06×10^{-13}	≈ 1 [a)]	≈ 0.3	(Boy et al., 2013)
Moderately polluted	Tarrant County, TX, Dallas−Fort Worth area June 2011	0.3 [a)]	-	1.3×10^{-12}	≈ 2 [a)]	< 0.43	(Kim et al., 2015)

[a)] Estimated from presented data; [b)] median; [c)] mean [d)] mean taken from (Novelli et al., 2017); [e)] nucleation events

S2 Experimental setup

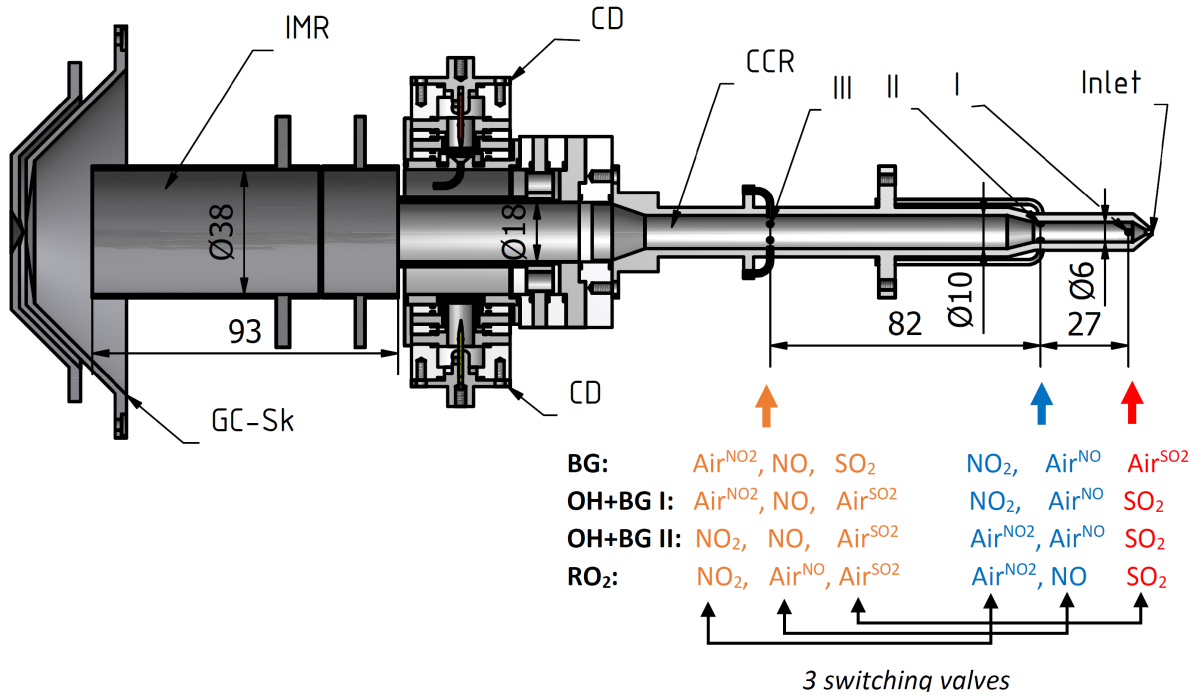

Figure S1. Schema of the reactor comprising a sampling inlet, the chemical conversion reactor (CCR), the ion molecule reactor (IMR), the NO_2/Air or NO_2/N_2 corona discharge ion sources (CD) and a gas curtain / skimmer assembly (GC-Sk). Positions of the three injector assemblies are shown as I, II and III. The 3 switching valves are used to interchange the two inlet positions between the flows of NO_2, SO_2 and NO reactant mixtures and the corresponding equal flows of pure air Air^{NO2}, Air^{SO2} and Air^{NO}, respectively. Switching of the NO_2, SO_2 and NO inlet positions allows for measurements in the background mode (BG), the two different OH+BG modes (OH+BG I and OH+BG II) and the (RO_2) mode. OH signal is derived from the difference of the signals measured in the OH+BG I or the OH+BG II and the BG modes. The OH+BG I and OH+BG II modes correspond to OH to H_2SO_4 chemical conversion times of 5 ms and 40 ms, respectively. Concentrations of SO_2, NO_2 and NO in the CCR are 3×10^{14} cm^{-3}, 1.2×10^{16} cm^{-3} and 3×10^{13} cm^{-3}, respectively, corresponding to OH consumption by SO_2 and NO_2 of about 4 ms and 7 µs, respectively. Additional NO_2 is added into the ion molecule rector via the ion source and with a flow of pure air sheath gas resulting in NO_2 concentration in the IMR of 5×10^{16} cm^{-3}. Presence time in the IMR is of 0.45 s. The reactor is made of stainless steel and Teflon isolation rings.

S3 Calibration of OH and H_2SO_4

Calibration of OH is performed by producing known concentrations of OH by photolysis of H_2O in air flow at λ=184.9 nm:

$H_2O + h\nu \rightarrow H + OH$

$H + O_2 + M \rightarrow HO_2 + M$

The generated in this way OH concentration is quantified by chemical actinometry using photolysis of N_2O at λ=184.9 nm producing NO of measurable concentrations. Calibration system is based on the same principles that have been previously described in the literature, (e.g. Dusanter et al., 2008; Kürten et al., 2012 and references therein). Below is given a detailed description of the calibration setup employed during the ChArMEx campaign in July-August 2013. This calibration system differs in several respects from the previously described calibration systems.

Measured signals I^{OH} and $I^{H_2SO_4}$ (see below) are related to OH and H_2SO_4 concentrations via calibration coefficients C_{OH} and $C_{H_2SO_4}$:

$$[OH] = C_{OH} \times I^{OH} \quad \text{(S1)}$$

$$[H_2SO_4] = C_{H_2SO_4} \times I^{H_2SO_4}; \quad C_{H_2SO_4} = C_{SA} \cdot C_{OH} \quad \text{(S2)}$$

In the following we describe the calibration setup and methods used to derive I^{OH} and $I^{H_2SO_4}$ signals and to estimate C_{OH}, $C_{H_2SO_4}$ and C_{SA} coefficients.

S3.1 Calibration setup

Essential elements of the calibration setup are presented in Figure S2. The whole setup is fixed on a frame allowing its placement in front of the instrument sampling aperture during field measurements or in a laboratory.

The photolysis of H_2O or N_2O is performed in a turbulent flow of humidified air or of N_2O/N_2 mixtures, respectively, passing through a photolysis reactor cell (11) (Figure S2). The photolysis reactor cell of 50 mm in length makes a segment of a calibration stainless steel flow tube (2) of diameter 18 mm. The rectangular volume illuminated by a mercury lamp (7) (Pen-Ray Lamp 11SC-1, UVP) is restricted by two 50 mm x 8 mm Heraeus Quarzglas Suprasil windows (10) fixed at a distance of 18 mm between them. The light from the Pen-Ray is passing through a 185 nm narrowband Acton Research 185-N filter (8) (0.1% transmission at 254 nm; 18% transmission at 185 nm) and through an adsorption cell (9) of length 3 cm which is fleshed either with N_2O/N_2 mixtures or with pure nitrogen allowing to vary the 184.9 nm light intensity in the photolysis cell. Inner volume of the adsorption cell is divided into parallel channels of 4x4 mm to reduce the light divergence. The light intensities on the exit from the photolysis cell and near the Pen-Ray lamp are monitored with two Hamamatsu R5764 phototubes (6) using homemade power supply and acquisition electronics. An enclosure surrounding the photolysis cell and other optical components as well as the compartment holding the Pen-Ray are flushed with nitrogen to avoid ozone formation.

The length of the flow tube section (2) between the photolysis cell and the end of the flow tube placed in front of the instrument sampling aperture (1) is variable from 5 cm to 35 cm in step of 5 cm to allow measurements of OH and H_2SO_4 wall loss rates (see below).

The humidified air or N_2O/N_2 mixtures at flow rate of 24-40 slm (*Re*=1800-3000) are introduced into the inlet flow tube (4) via an entrance section (5) containing humidity and temperature sensors (Michell Instruments Optidew chilled mirror hygrometer and Vaisala capacitive DRYCAP dewpoint and temperature transmitter DMT340/347). The flow rates are controlled with Bronkhorst EL-FLOW mass flow controllers. Water is added to the flow of air using Bronkhorst water mass flow controllers (LIQUI-FLOW 24 g/h and μ-FLOW 1.4g/h). Addition of SO_2 (5% SO_2/Air, Air Liquide) for H_2SO_4 calibration can be made either before the entrance section or after the photolysis cell via an injector in the end section of the flow tube. In-field calibration was usually performed using air and nitrogen ALPHAGAZ 2 and N_2O N48 gases (Air Liquid).

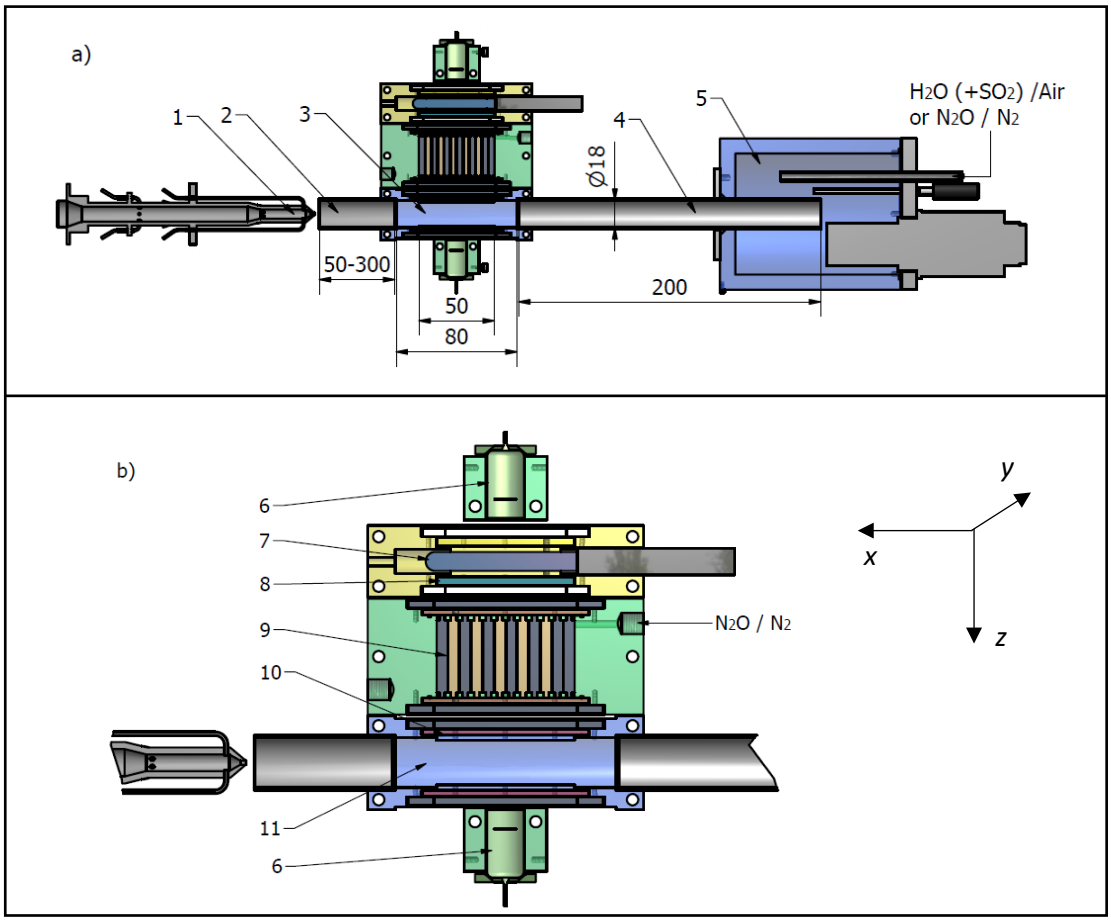

Figure S2. Schema of the calibration setup (a) and detailed view of the photolysis cell (b): 1 - inlet of CIMS; 2 – calibration flow tube; 3 – photolysis cell; 4 – inlet flow tube; 5 – entrance volume with temperature and humidity sensors; 6 – phototubes; 7 – Hg Pen-Ray lamp; 8 – bandpass filter; 9 – N_2O absorption cell; 10 – windows; 11 – photolysis reactor cell.

S3.2 Estimation of OH and H_2SO_4 concentrations produced by calibration setup

Accounting for a fast turbulent mixing in the flow tube the concentration of OH on the exit of the photolysis cell is:

$$[\mathrm{OH}] = \frac{1}{S}\iint_{y,z}\left(\int_0^L \psi(x,y,z)\sigma_{\mathrm{H_2O}}[\mathrm{H_2O}]\frac{dx}{v(x,y,z)}\right)\cdot dy\cdot dz \qquad \text{(S3)}$$

Here, $\psi(x,y,z)$ and $v(x,y,z)$ are photon flux and flow velocity at point *x, y, z* of the photolysis cell (Figure S2), respectively, $\sigma_{\mathrm{H_2O}}$ is the absorption cross section of water at 184.9 nm, *S* is the area of the tube section in *y, z* plane excluding viscous sublayer and integration is over *y, z* of the illuminated region, also excluding viscous sublayer.

Assuming that all light rays are parallel in z direction, one can separate the dependence of ψ on *z* and *x, y* accounting for the attenuation of the light at wavelength of 184.9 nm due to the adsorption by water and oxygen:

$$\psi(x,y,z) = \psi_0(x,y)\exp(-\left(\sigma_{\mathrm{H_2O}}[\mathrm{H_2O}] + \sigma_{\mathrm{O_2}}[\mathrm{O_2}]\right)\cdot z) \qquad \text{(S4)}$$

Also, assuming a flatness of the flow velocity profile in the turbulent core and assuming that the flow velocity is independent on *x* and *y* (the width of illuminated volume in the cell is 8 mm compared to the tube diameter of 18 mm) we obtain:

$$[\mathrm{OH}] = \frac{1}{S} \times \sigma_{\mathrm{H_2O}} [\mathrm{H_2O}] \times \Psi_0^{\mathrm{OH}} \times \int_0^{D_{turb}} \frac{\exp(-(\sigma_{\mathrm{H_2O}} [\mathrm{H_2O}] + \sigma_{\mathrm{O_2}} [\mathrm{O_2}]) \cdot z)}{v(z)} \cdot dz \quad \text{(S5)}$$

Here, $\Psi_0^{\mathrm{OH}} = \iint_{y,z} \psi_0(x,y) \cdot dy \cdot dz$ is the incident photon flux integrated over the entrance window area, D_{turb} is the distance between the entrance and exit windows of the cell excluding viscous sublayer.

In case of N_2O photolysis one can write a similar expression for the NO concentration:

$$[\mathrm{NO}] = \frac{1}{S} \times \sigma_{\mathrm{N_2O}} [\mathrm{N_2O}] \times f(\mathrm{N_2O}) \times \Psi_0^{\mathrm{N_2O}} \times \int_0^{D_{turb}} \frac{\exp(-\sigma_{\mathrm{N_2O}} [\mathrm{N_2O}] \cdot z)}{v(z)} \cdot dz \quad \text{(S6)}$$

Here, $f(N_2O)$ is the yield of NO per one photon absorbed by N_2O according to the reaction mechanism (SR0-SR3, see Table S2):

$$f(\mathrm{N_2O}) = {2k_{3a}[\mathrm{N_2O}]} \Big/ {k_1[\mathrm{O_2}] + k_2[\mathrm{N_2}] + k_3[\mathrm{N_2O}]} \quad \text{(S7)}$$

$N_2O + h\nu$	$\rightarrow$	$N_2 + O(^1D)$	(SR0)
$O(^1D) + O_2$	$\rightarrow$	$O(^3P) + O_2$	(SR1)
$O(^1D) + N_2$	$\rightarrow$	$O(^3P) + N_2$	(SR2)
$O(^1D) + N_2O$	$\rightarrow$	$NO + NO$	(SR3a)
	$\rightarrow$	$N_2 + O_2$	(SR3b)
	$\rightarrow$	$O(^3P) + N_2O$	(SR3c)

As the flow conditions are the same for H_2O and N_2O photolysis we can relate the NO and OH concentrations as:

$$\frac{[\mathrm{OH}]}{[\mathrm{NO}]} = \frac{\Psi_0^{\mathrm{OH}}}{\Psi_0^{\mathrm{NO}}} \frac{\sigma_{\mathrm{H_2O}}}{\sigma_{\mathrm{N_2O}}} \frac{[\mathrm{H_2O}]}{[\mathrm{N_2O}] \cdot f(\mathrm{N_2O})} \times \left\{ \frac{\int_0^{D_{turb}} \frac{\exp(-(\sigma_{\mathrm{H_2O}} [\mathrm{H_2O}] + \sigma_{\mathrm{O_2}} [\mathrm{O_2^{H_2O}}]) \cdot z)}{v(z)} \cdot dz}{\int_0^{D_{turb}} \frac{\exp(-\sigma_{\mathrm{N_2O}} [\mathrm{N_2O}] \cdot z)}{v(z)} \cdot dz} \right\} \quad \text{(S8)}$$

To evaluate the ratio of the integrals in (S8) we farther approximate the flow velocity profile of the turbulent core in z direction by a flat profile of a plug flow:

$$[\mathrm{OH}] = \frac{[\mathrm{NO}]}{f(\mathrm{N_2O})} \times \frac{\sigma_{\mathrm{H_2O}} [\mathrm{H_2O}]}{\sigma_{\mathrm{H_2O}} [\mathrm{H_2O}] + \sigma_{\mathrm{O_2}} [\mathrm{O_2^{H_2O}}]} \times \frac{\Psi_0^{\mathrm{OH}} \left(1 - \exp\left(-(\sigma_{\mathrm{H_2O}} [\mathrm{H_2O}] + \sigma_{\mathrm{O_2}} [\mathrm{O_2^{H_2O}}]) D\right)\right)}{\Psi_0^{\mathrm{NO}} \left(1 - \exp\left(-(\sigma_{\mathrm{N_2O}} [\mathrm{N_2O}]) D\right)\right)} \quad \text{(S9)}$$

In (S9), we neglect an influence of the viscous sublayer of thickness of about 1 mm at our flow conditions and assume that the absorption length is equal to the distance between the entrance and exit windows of the cell, $D_{turb} \approx D$. The error of the ratio of the integrals in (S8) evaluated using the plug flow approximation is less than 1% for N_2O volume fraction less than 0.5. This was found by comparing the approximated and the numerically calculated integrals using turbulent flow velocity profile consisting of viscous sublayer (y+<5), buffer layer (5<y+<30) and logarithmic low region (y+>30) (Tennekes and Lumley, 1972).

Finally, accounting for first order losses of OH (e.g. wall loss or reactions with impurities) and using the proportionality of the total photon flux and the measured phototube current we obtain for the OH concentration at the exit of the flow tube:

$$[\mathrm{OH}] = \frac{I_{185}\left(\exp\left(\left(\sigma_{\mathrm{H_2O}}[\mathrm{H_2O}] + \sigma_{\mathrm{O_2}}\left[\mathrm{O_2}\right]\right)D\right) - 1\right)}{1 + \frac{\sigma_{\mathrm{O_2}}\left[\mathrm{O_2}\right]}{\sigma_{\mathrm{H_2O}}[\mathrm{H_2O}]}} \times C_{\mathrm{N_2O}} \times C_{loss}^{cell} \times C_{loss}^{tube} \quad \text{(S10)}$$

Where, I_{185} is the phototube current proportional to the total photon flux at 184.9 nm (see comment in section 3.4.2) on the exit of the photolysis reactor cell and $C_{\mathrm{N_2O}}$ is the calibration coefficient derived from the yield of NO in the photolysis of N_2O:

$$C_{\mathrm{N_2O}} = \frac{[\mathrm{NO}]}{\Delta I^{\mathrm{NO}} \times f(\mathrm{N_2O})} \quad \text{(S11)}$$

Here, ΔI^{NO} is the difference of the phototube current in absence and in presence of N_2O and $f(N_2O)$ is the yield of NO by photolysis of N_2O defined above by the equation (S7).

The correction coefficients C_{loss}^{cell} and C_{loss}^{tube} accounting for a first order loss of OH in the cell and in the flow tube, respectively, can be easily derived from differential equation describing OH production and the first order loss:

$$C_{loss}^{cell} = \left(\frac{1 - \exp\left(-K_{\mathrm{OH}} \cdot t_{cell}\right)}{K_{\mathrm{OH}} \cdot t_{cell}}\right) \quad \text{(S12)}$$

$$C_{loss}^{tube} = \exp\left(-K_{\mathrm{OH}} \cdot t\right) \quad \text{(S13)}$$

In (S12) and (S13), K_{OH} is a first order OH loss rate coefficient, t_{cell} and t are the presence times in the cell and in the flow tube end section, respectively, calculated from corresponding lengths and bulk flow velocity. In absence of SO_2 being added to the flow for H_2SO_4 calibration the OH loss is explained predominantly by the wall losses, $K_{\mathrm{OH}} = K_{\mathrm{OH}}^{W}$.

Estimation of OH concentration according to (S10) is made using measured phototube current and H_2O concentration, with other parameters $C_{\mathrm{N_2O}}$, C_{loss}^{cell}, C_{loss}^{tube} being determined in separate experiments. It is important to note that calibration of the phototube is not required. It is essential, however, that sensitivity of the phototube remains unchanged after determination of $C_{\mathrm{N_2O}}$.

For H_2SO_4 calibration OH is converted to H_2SO_4 by adding SO_2 to the flow tube. In this case OH concentration is also described by (S10), but with OH loss coefficient taking into account OH wall loss and OH consumption in the reaction of OH with SO_2:

$$K_{\mathrm{OH}} = K_{\mathrm{OH}}^{W} + k_{\mathrm{OH+SO_2}} \cdot [\mathrm{SO_2}] \quad \text{(S14)}$$

Solving differential equation for H_2SO_4 accounting for H_2SO_4 production in the reaction of OH with SO_2 and its first order loss on the walls of the flow tube we obtain:

$$[\mathrm{H_2SO_4}] = [\mathrm{OH}] \times k_{\mathrm{OH+SO_2}} \cdot [\mathrm{SO_2}] \cdot \frac{e^{(K_{\mathrm{OH}} - K_{\mathrm{SA}}) \cdot t}}{\left(1 - e^{-K_{\mathrm{OH}} \cdot t_{cell}}\right)} \cdot \left(\frac{1}{K_{\mathrm{SA}}} - \frac{K_{\mathrm{OH}} e^{-K_{\mathrm{SA}} \cdot t_{cell}}}{K_{\mathrm{SA}}\left(K_{\mathrm{OH}} - K_{\mathrm{SA}}\right)} + \frac{1 + e^{K_{\mathrm{SA}} \cdot t} e^{-K_{\mathrm{OH}}\left(t_{cell} + t\right)} - e^{(K_{\mathrm{SA}} - K_{\mathrm{OH}}) \cdot t}}{\left(K_{\mathrm{OH}} - K_{\mathrm{SA}}\right)}\right) \quad \text{(S15)}$$

Where [OH] is the OH concentration described by (S10) with K_{OH} according to (S14) and K_{SA} is the H_2SO_4 first order wall loss rate coefficient.

Photodissociation of SO_2 at 184.9 nm may lead to SO_3 and, hence, additional H_2SO_4 formation according to the reactions (SR4 – SR6). This contribution is higher for higher ratio of $[SO_2]$ to $[H_2O]$. Using the listed here rate coefficients and SO_2 photodissociation cross section the maximum contribution to H_2SO_4 formation from the SO_2 photolysis was estimated to be about 0.8% at relative humidity of 10% and SO_2 concentration of 5×10^{13} cm^{-3}. In all calibration experiments the ratio $[SO_2]/[H_2O]$ was maintained low enough to keep the contribution of SO_2 photodissociation to H_2SO_4 formation lower than 1%.

$SO_2 + h\nu \rightarrow SO + O$ (SR4) 3.11×10^{-18} cm^2 (Danielache et al., 2008).

$O + SO_2 + M \rightarrow SO_3 + M$ (SR5) 1.3×10^{-14} cm^3 molecule^{-1} s^{-1} (Burkholder et al., 2015)

$SO + O_2 \rightarrow SO_2 + O$ (SR6a) 7.6×10^{-17} cm^3 molecule^{-1} s^{-1} (Atkinson et al., 2004)

$SO + O_2 + M \rightarrow SO_3 + M$ (SR6b) $< 10^{-36}$ cm^6 molecule^{-2} s^{-1} (Black et al., 1982), (Whitehill et al., 2015)

At maximum used SO_2 concentration of 5×10^{13} cm^{-3} attenuation of light at 184.9 nm by SO_2 can be neglected.

S3.3 Mass peaks intensities and OH, H_2SO_4 concentrations

To distinguish ambient H_2SO_4 and H_2SO_4 produced by chemical conversion of OH the conversion is performed with $^{34}SO_2$ added into the CCR of the CIMS instrument. OH and H_2SO_4 are derived from measurement of peak intensities I_{62} (m/z=62, NO_3^-), I_{97} (m/z=97, $H^{32}SO_4^-$) and I_{99} (m/z=99, $H^{34}SO_4^-$). Accounting for the isotopic composition of SO_2 used for the chemical conversion (99% isotopic enrichment of ^{34}S, EURISO-TOP) and sulphur and oxygen isotope natural abundance (94% and 5% for HSO_4 m/z=97 and m/z=99, respectively) the measured I_{62}, I_{97} and I_{99} are related to OH and H_2SO_4 concentrations as follows:

$$I_{97} / I_{62} = 0.94 \cdot \frac{1}{C_{\mathrm{H_2SO_4}}} \cdot [\mathrm{H_2SO_4}] + \frac{1}{C_{\mathrm{OH}}} \cdot \left(\frac{0.01 \cdot [\mathrm{SO_2}]^{CCR} + 0.94 \cdot [\mathrm{SO_2}]^{Ext}}{[\mathrm{SO_2}]^{CCR} + [\mathrm{SO_2}]^{Ext}} \right) \cdot [\mathrm{OH}] \quad \text{(S16)}$$

$$I_{99} / I_{62} = 0.05 \cdot \frac{1}{C_{\mathrm{H_2SO_4}}} \cdot [\mathrm{H_2SO_4}] + \frac{1}{C_{\mathrm{OH}}} \cdot \left(\frac{0.99 \cdot [\mathrm{SO_2}]^{CCR} + 0.05 \cdot [\mathrm{SO_2}]^{Ext}}{[\mathrm{SO_2}]^{CCR} + [\mathrm{SO_2}]^{Ext}} \right) \cdot [\mathrm{OH}] \quad \text{(S17)}$$

Here, indexes *FT* and *CCR* indicate concentrations of SO_2 in the calibration flow tube reactor (or ambient concentration of SO_2) and in the CCR, respectively. C_{OH} and $C_{\mathrm{H_2SO_4}}$ are the calibration coefficients defined by (S1) and (S2). Then, combinations of I_{97} and I_{99} corresponding to OH and H_2SO_4 concentrations are calculated as follows:

$$I^{OH} = \frac{1}{C_{\mathrm{OH}}} \cdot [\mathrm{OH}] = \frac{\left(\frac{I_{99}}{I_{62}} - \frac{0.05}{0.94} \cdot \frac{I_{97}}{I_{62}} \right)}{\left(0.99 - 0.01 \cdot \frac{0.05}{0.94} \right)} \cdot \left(1 + \frac{[\mathrm{SO_2}]^{Ext}}{[\mathrm{SO_2}]^{CCR}} \right) \quad \text{(S18)}$$

$$I^{\mathrm{H_2SO_4}} = \frac{1}{C_{\mathrm{H_2SO_4}}} \cdot [\mathrm{H_2SO_4}] = \frac{1}{0.94} \cdot \frac{I_{97}}{I_{62}} - \frac{\left(\frac{I_{99}}{I_{62}} - \frac{0.05}{0.94} \cdot \frac{I_{97}}{I_{62}} \right)}{\left(0.99 - 0.01 \cdot \frac{0.05}{0.94} \right)} \cdot \left(\frac{0.01}{0.94} + \frac{[\mathrm{SO_2}]^{Ext}}{[\mathrm{SO_2}]^{CCR}} \right) \quad \text{(S19)}$$

For ambient measurements, when $\frac{[\mathrm{SO_2}]^{Ext}}{[\mathrm{SO_2}]^{CCR}}$ is typically less than 10^{-4}, (S18) and (S19) can be simplified:

$$I^{OH} = \frac{1}{0.99} \cdot \frac{I_{99}}{I_{62}} - \frac{0.05}{0.99 \cdot 0.94} \cdot \frac{I_{97}}{I_{62}} \quad \text{(S20)}$$

$$I^{\mathrm{H_2SO_4}} = \frac{1}{0.94} \cdot \frac{I_{97}}{I_{62}} - \frac{0.01}{0.99 \cdot 0.94} \cdot \frac{I_{99}}{I_{62}} \quad \text{(S21)}$$

S3.4 Calibration example

S3.4.1 OH and H_2SO_4 wall loss rates

The wall loss rate coefficients are determined by measuring the dependence of OH or H_2SO_4 signal intensities on the length of the end section of the flow tube (varied from 5 cm to 35 cm with a step of 5 cm (Figure S3). High concentration of SO_2, in these experiments, of up to 5×10^{14} cm^{-3}, was used for fast conversion of OH into H_2SO_4.

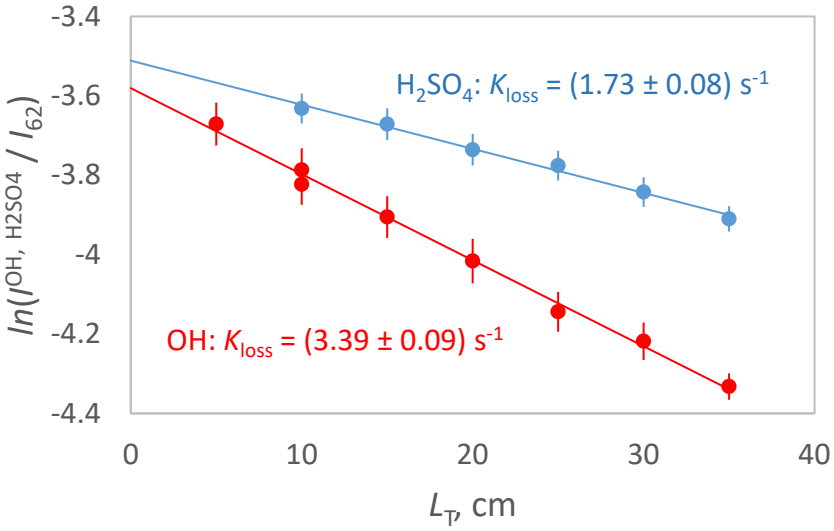

Figure S3. Example of wall loss decay rate measurements: red - OH decay at RH=43%; blue - H_2SO_4 decay at RH=45% and $[SO_2]$ =5×10^{14} cm^{-3}.

S3.4.2 Determination of C_{N_2O} from N_2O photolysis

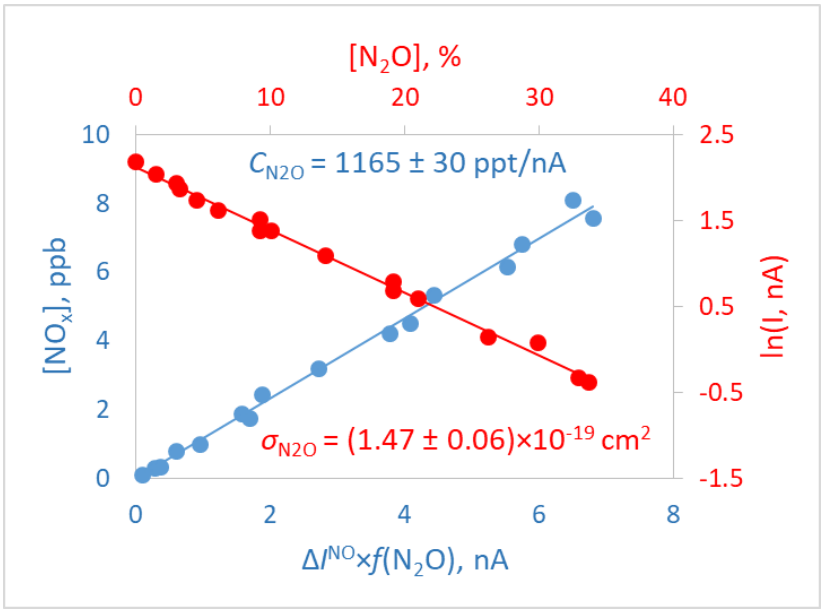

Figure S4. Determination of the calibration coefficient C_{N_2O} by measuring $[NO_x]$ from the photolysis of N_2O at 184.9 nm as a function on $\Delta I^{NO} \times f(N_2O)$ (blue points). Red points represent dependence of the phototube current on N_2O concentration. Absorption cross section of N_2O obtained from this dependence is in agreement with the literature value of 1.43×10^{-19} cm^2 (Creasey et al., 2000).

NO generated by N_2O photolysis was measured using Ecotech EC9841T NOx Trace Analyser. The lower detection limit of this analyser was estimated to be about 100 ppt (10 min integration time, 1σ at S/N=1). To produce sufficient NO concentrations the N_2O photolysis was conducted without the 185 nm bandpass filter, while the production of OH by the photolysis of H_2O was performed with the filter installed to allow using of water vapour concentrations high enough for a reliable H_2O measurements. In both cases the contribution of the strongest emission line of the mercury Pen-Ray lamp at 254 nm to the measured with the phototube photocurrent was not negligible. As the absorption by N_2O at 254 nm is negligible, this contribution was determined from the dependence of the photocurrent on the concentration of N_2O in the absorption cell of the calibrator and was found to be of (56±2)% and of (5.10±0.05)% for the configurations without and with filter, respectively (during the ChArMEx campaign).

S3.4.3 Calibration of OH and H_2SO_4

In Figure S5 is presented an example of a typical calibration procedure consisting of measurement of dependences of I^{OH} and I^{H2SO4} defined in (S18) and (S19) on the photolysis light intensity and concentrations of H_2O and SO_2 in the calibration flow tube.

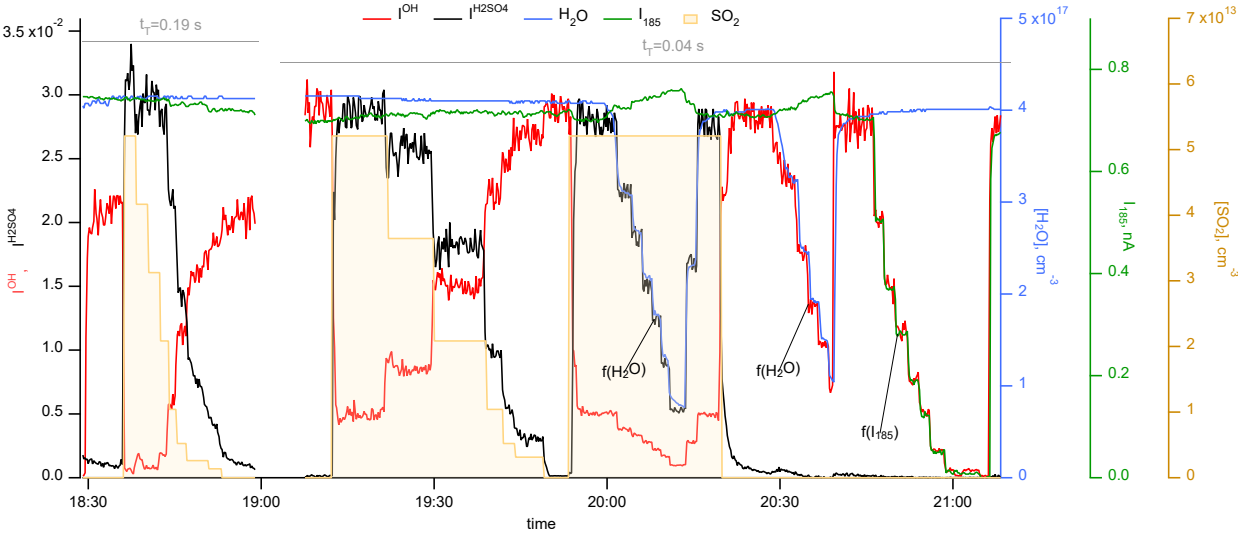

Figure S5. Example of "fast" field calibration of OH and H_2SO_4 including conversion of OH to H_2SO_4 at different SO_2 concentrations and dependencies of OH and H_2SO_4 signals on $[H_2O]$ and of OH signal on light intensity I_{185}. The conversion of OH to H_2SO_4 was conducted at two calibration reactor lengths corresponding to reaction time of 0.19 s and 0.04 s.

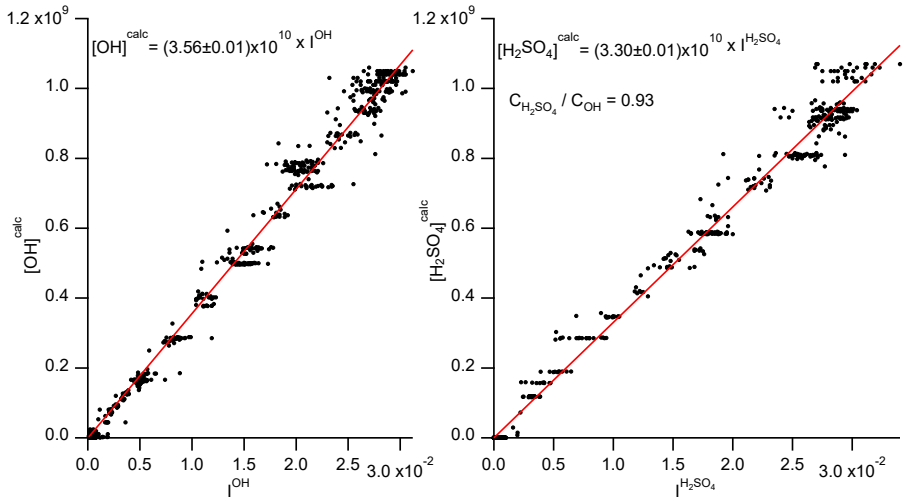

Figure S6. Comparison of all measured I^{OH} and I^{H2SO4} shown in Figure S4 with calculated [OH] and $[H_2SO_4]$.

The calibration coefficients C_{OH} and $C_{H_2SO_4}$ can be determined by comparing the measured I^{OH} and I^{H2SO4} with [OH] and [H_2SO_4] calculated according to (S10) and (S15), as shown in Figure S6 and Figure S7.

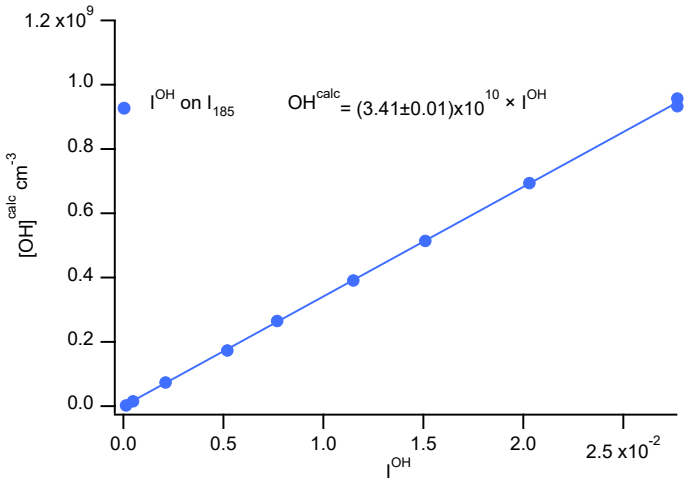

Figure S7. Example of OH calibration coefficient determination from the dependence of I^{OH} on light intensity using data presented in Figure S5.

In practice, the calibration coefficient C_{OH} is determined in absence of SO_2 (e.g. as shown in Figure S7) while the ratio C_{SA} =C_{H2SO4}/C_{OH} is determined by fitting measured ratios of $I^{H2SO4}/\Delta I^{OH}$ to the calculated ratios of [H_2SO_4]/Δ[OH] at different $[SO_2]^R$, as shown in Figure S8. Δ[OH] and ΔI^{OH} correspond to a difference of the calculated [OH] and the measured I_{OH}, respectively, in absence and presence of SO_2. Determined in this way, the C_{OH} calibration coefficient is independent on the value used for the OH+SO_2 rate coefficient while the ratio C_{SA} =C_{H2SO4}/C_{OH} is independent on the sensitivity to OH and only slightly depends on the value of the k_{OH+SO2} as shown in Figure S8.

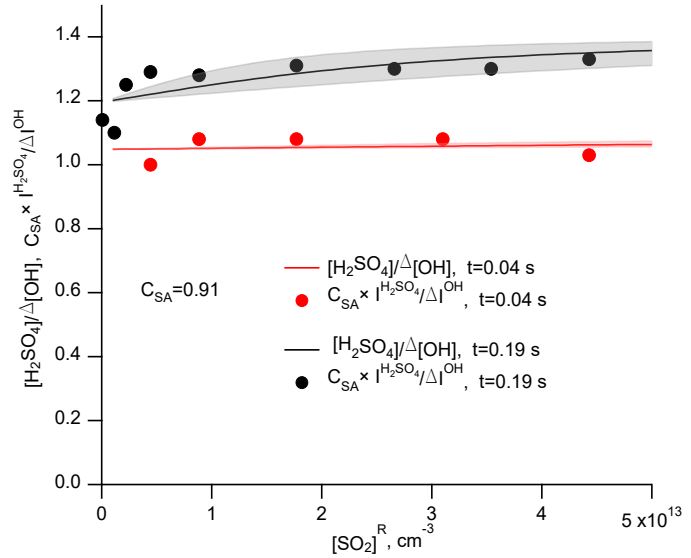

Figure S8. Calibration of relative sensitivity of OH and H_2SO_4: dependencies of calculated (lines) and measured (dots) ratios of the generated H_2SO_4 to the OH consumption on the SO_2 concentration in the calibration flow tube reactor. Red and black colors correspond to the shorter and the longer flow tubes, respectively. Shadowed gray and red regions show sensitivity to the used rate coefficient of the reaction OH+SO_2: upper and lower boundaries correspond to the rate constant multiplied and divided by 2. Larger ratio of H_2SO_4 to ΔOH at the shorter reaction time is explained by faster wall loss of OH compared to H_2SO_4.

S3.5 Photochemical coefficients and uncertainty estimation.

Table S2. Photochemical coefficients used for the calculation of OH and H_2SO_4

Parameter	Value	Uncertainty (1σ)	Reference
σ_{H_2O}	$(7.22\pm0.22)\times10^{-20}$ cm^2	3%	(Creasey et al., 2000)
σ_{O_2}	$(1.14\pm0.05)\times10^{-20}$ cm^2	5%	(Creasey et al., 2000)
σ_{N_2O}	$(1.43\pm0.02)\times10^{-19}$ cm^2	2%	(Creasey et al., 2000)
SR1, k_1	$3.3\times10^{-11}exp(-55/T)$ cm^3 s^{-1}	10%	(Sander et al., 2011)
SR2, k_2	$2.5\times10^{-11}exp(-110/T)$ cm^3 s^{-1}	10%	(Sander et al., 2011)
SR3, k_3	$1.19\times10^{-10}exp(-20/T)$ cm^3 s^{-1}	10%	(Sander et al., 2011)
SR3a, k_{3a}	$7.25\times10^{-11}exp(-20/T)$ cm^3 s^{-1}	10%	(Sander et al., 2011)
k_{OH+SO2}	8.06×10^{-13} cm^3 s^{-1} (760 torr, 298K)	25% *)	(Atkinson et al., 2004)

*) estimated (see discussion in the article)

Table S3. Estimation of uncertainties

	Range of values	Estimated uncertainty (1σ)
Absorption length D due to light divergence	18 mm	5%
Plug flow approximation		1%
I_{185}, (photocurrent corresponding to 184.9 nm with correction for 254 nm contribution)	0.01 – 1, nA	5%
$[H_2O]$	$(0.5 – 7)\times10^{17}$, cm^{-3}	5% a)
$[SO_2]$	$(10^{-4} – 10)\times10^{14}$, cm^{-3}	5% b)
C_{N2O} (NO, $f(N_2O)$)	1100 – 1200, ppt nA^{-1}	20% c)
K_{OH} (wall loss at $[SO_2]^R=0$)	2 – 3.5, s^{-1}	10%
K_{H2SO4}	1 – 2.5, s^{-1}	10%
Wall losses correction for OH	0.87 – 0.93 d)	10%
$[OH]^{calc}$		25%
$[H_2SO_4]^{calc}$		35% e)
C_{OH}	$(3.4 – 3.6)\times10^{10}$	30%
C_{H2SO4}	$(3.4 – 3.6)\times10^{10}$	40% e)
$C_{SA}= C_{H2SO4} / C_{OH}$	0.9-0.95	8% f)
Resulting calibration uncertainties		
[OH], cm^{-3}	2×10^5 - 2×10^9	30%
$[H_2SO_4]$, cm^{-3}	1×10^5 - 2×10^9	32% g)
$[H_2SO_4]$ / [OH]	$10^{-4} – 10^4$	8% g)

a) With Michell Instruments Optidew chilled mirror hygrometer
b) Using SO_2 monitor TELEDYNE T100U
c) Uncertainties of NO, $f(N_2O$ and ΔI^{NO} are 10%, 15%, 10%, respectively
d) At flow tube length of 5 cm
e) Using $H_2SO_4^{calc}$ from (S15)
f) Using the method shown in Figure S8
g) Using C_{SA}

S4 Estimation of H_2SO_4 production in reactions of SCIs with SO_2

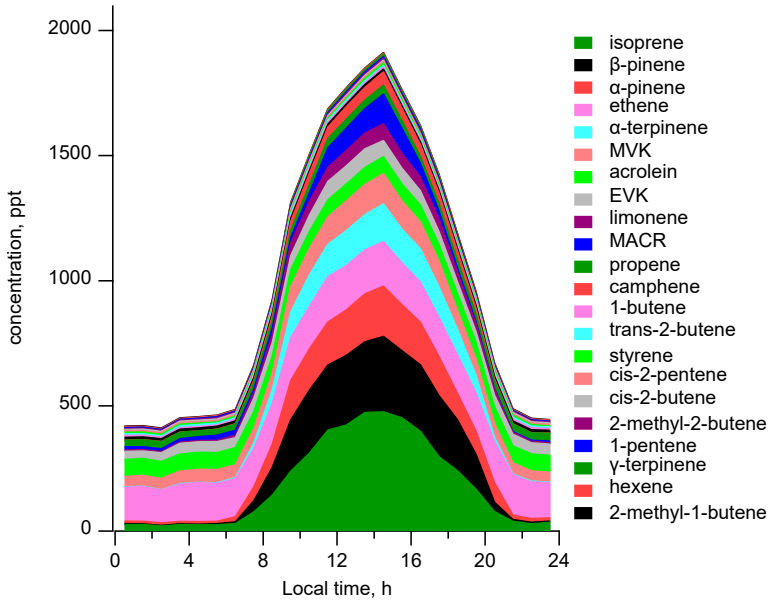

Figure S9. Median diel concentration profiles of observed unsaturated VOCs

Table S4. Measured unsaturated VOCs and the corresponding measurement techniques, VOCs+O_3 reaction rate coefficients (k_{VOC+O3}), specific yields of Criegee Intermediates (CI) (Y_{SCI}) and yields of stabilized CIs (SCIs) (α_{SCI})

	VOC	Method	Median (ppt) Day (7 h-20 h) / Night (20 h – 7 h)	k_{VOC+O3} [a], 10^{-17} $cm^3 molecule^{-1} s^{-1}$	Yield of stabilized SCI α_{SCI} [b]		SCI: (R1) – (R2) COO / CI specific yield Y_{SCI} [b]
1	Ethene	A	167 / 153	0.16	0.37	1	CH_2OO / 1
2	Propene	A	31 / 28	1.0	0.37	1 2 3	CH_2OO / 0.5 [c] $-CH_3$ -H / 0.4 [c] -H $-CH_3$ / 0.1 [c]
3	1-Butene	A	7 / 7	1.0	0.4	1 4 5	CH_2OO / 0.5 $-CH_2R_a$ -H / 0.4 -H $-CH_2R_a$ / 0.1
4	*trans*-2-Butene	A	7 / 7	19	0.4	2 3	$-CH_3$ -H / 0.8 -H $-CH_3$ / 0.2
5	*cis*-2-Butene	A [1]	5	13	0.38	2 3	$-CH_3$ -H / 0.8 -H $-CH_3$ / 0.2
6	2-Methyl-1-butene	A [1]	2	1.4 [d]	0.4	1 6 7	CH_2OO / 0.5 $-CH_2R_a$ $-CH_3$ / 0.25 $-CH_3$ $-CH_2R_a$ / 0.25
7	2-Methyl-2-butene	A [3]	6 / 4	40 [e]	0.4	2 3 8	$-CH_3$ -H / 0.4 -H $-CH_3$ / 0.1 $-CH_3$ $-CH_3$ / 0.5
8	*trans*-2-Pentene	A [1]	11	16 [d]	0.4	2 3 4 5	$-CH_3$ -H / 0.4 -H $-CH_3$ / 0.1 $-CH_2R_a$ -H / 0.4 -H $-CH_2R_a$ / 0.1
9	*cis*-2-Pentene	A [1]	6 / 6	13 [d]	0.29	2 3 4 5	$-CH_3$ -H / 0.4 -H $-CH_3$ / 0.1 $-CH_2R_a$ -H / 0.4 -H $-CH_2R_a$ / 0.1
10	1-Pentene	A [3]	6 / 4	0.9 [d]	0.29	1 4 5	CH_2OO / 0.5 $-CH_2R_a$ -H / 0.4 -H $-CH_2R_a$ / 0.1
11	1-Hexene	B [1]	4 / 4	1.0 [d]	0.4	1 4 5	CH_2OO / 0.5 $-CH_2R_a$ -H / 0.4 [g] -H $-CH_2R_a$ / 0.1 [g]

12	Isoprene	C,D	355 / 32	1.3	0.95 [f] 0.34 [f] 0.54 [f] 0.37 [f] 0.2 [f]	1 9 10 11 12	CH_2OO / 0.33 [f] Z-($CH=CH_2$)(CH_3)COO / 0.21 [f] (MVK oxide) E-($CH=CH_2$)(CH_3)COO / 0.26 [f] Z-($C(CH_3)=CH_2$)CHOO / 0.02 [f] (MACR-oxide) E-($C(CH_3)=CH_2$)CHOO / 0.2 [f]
13	α-pinene	B	162 / 13	9.6	0.15	13 14 15 16	Z-pinonaldehyde-K-oxide / 0.25 E-pinonaldehyde-K-oxide / 0.25 Z-pinonaldehyde-A-oxide / 0.25 E-pinonaldehyde-A-oxide / 0.25
14	β-pinene	B	247 / 6	1.9	0.5	1 17 18	CH_2OO / 0.1 Z-Nopinone oxide / 0.77 E-Nopinone oxide / 0.13
15	Camphene	B	44 / 1	0.05	0.5 [h]	1 19 20	CH_2OO / 0.5[g] -$CRaRbRc$ -$CHRdRe$ / 0.25 [g] - $CHRdRe$ -$CRaRbRc$ / 0.25 [g]
16	Limonene	B	53 / 7	22	0.27	1 4 5 6 7 21 22	CH_2OO / 0.11 -CH_2R_a -H / 0.31 -H -CH_2R_a / 0.08 -CH_2R_a -CH_3 / 0.195 -CH_3 -CH_2R_a / 0.195 -CHR_aR_b -CH_3 / 0.055 - CH_3 -CHR_aR_b / 0.055
17	γ-terpinene	B	11 / 0	16	0.15	5 7 23 24 25 26	-H -CH_2R_a / 0.135+0.115 -CH_3 -CH_2R_a / 0.115 -CH_2-$CR_3=CR_4R_5$ –H / 0.135+0.115 -CH_2-$CR_3=CR_4R_5$ –CH_3 / 0.115 -CH_2-$CR_3=CR_4R_5$ –CHR_aR_b / 0.135 -CHR_aR_b –CH_2R_a / 0.135
18	α-terpinene	B	124 / 3	1900	0.15	6 7 26 27 28 29	-CH_2R_a -CH_3 / 0.125 -CH_3 -CH_2R_a / 0.125 -CHR_aR_b –CH_2R_a / 0.125 –CH_2R_a -CHR_aR_b / 0.125 -($CR_3=CR_4CH_3$) –H / 0.25 -H -($CR_3=CR_4CH_3$) / 0.25
19	Methyl vinyl ketone (MVK)	C & D [2]	102 / 45	0.52	0.4	1 30 31	CH_2OO / 0.5 -C(O)Ra –H / 0.25 -H -$C(O)R_3$ / 0.25
20	Ethyl vinyl ketone (EVK)	C	62 / 40	0.6 [g]	0.4	1 30 31	CH_2OO / 0.5 -C(O)Ra –H / 0.25 -H -$C(O)R_3$ / 0.25
21	Methacrolein (MACR)	C & D [2]	48 / 5	0.12	0.4	1 32 33	CH_2OO / 0.5 -C(O)H –CH_3 / 0.25 -CH_3 -$C(O)R_3$ / 0.25
22	Acrolein (Propenal)	E [1]	68	0.014 [g]	0.4	1 34 31	CH_2OO / 0.5 -C(O)H –H / 0.25 -H -$C(O)R_3$ / 0.25
23	Styrene	B & A [4]	8 / 6	1.4 [h]	0.4	1 35 36	CH_2OO / 0.5 -$CRaRbRc$ –H / 0.25 -H -$CRaRbRc$ / 0.25

A) Online GC-FID-FID; time resolution 90 min; LOD range 10-100ppt; uncertainty range 5-23%
B) Offline solid adsorption + GC FID; time resolution 180 min; LOD 5ppt; uncertainty range 25%
C) PTR MS; time resolution 10 min; LOD range 7-500ppt; uncertainty range 6-23%
D) Online GC-FID-MS; time resolution 90 min; LOD range 5-100ppt; uncertainty range 5-14%
E) DNPH-HPLC; time resolution 180 min; LOD range 6-40ppt; uncertainty range 25%
1) Averaged value was used
2) The sum of MVK and MACR measured by PTRMS the MVK measurements by online GC-FID-MS
3) From the sum of 1-Pentene and 2-Methyl-2-butene (taken 1 to 1)
4) combined data from GC-FID and SA-GC-FID
a) All the rate constants are from (Atkinson et al., 2006; IUPAC, 2020) except indicated otherwise
b) SCIs naming convention and Y_{SCI} are from (Vereecken et al., 2017 and references therein), except indicated otherwise
c) (Novelli et al., 2014)
d) (Avzianova and Ariya, 2002)
e) (Witter et al., 2002)
f) (Zhang et al., 2002)
g) (Grosjean et al., 1993)
h) (Le Person et al., 2008)

Table S5. SCIs derived from observed unsaturated VOCs, their precursor VOCs and their rate coefficients for thermal decomposition and reactions with H_2O and $(H_2O)_2$ [*)]

	SCI	K, [A)] s^{-1}	k_{H2O}, [A) B)] $cm^{-3}\ s^{-1}$	$k_{(H2O)2}$, [A) B)] $cm^{-3}\ s^{-1}$	k_{SO2}, $cm^{-3}\ s^{-1}$	Precursor
1	CH_2OO	0.3	8.7×10^{-16} (**435**)	1.4×10^{-12} (**700**)	3.7×10^{-11}	Ethene, propene, 1-Butene, 2-Methyl-1-butene, 1-pentene, 1-hexene, isoprene, β-pinene, camphene, limonene, MVK, EVK, MACR, acrolein, styrene
2	Z-$(CH_3)CHOO$	**136**	6.7×10^{-19} (0.3)	2.3×10^{-14} (12)	2.7×10^{-11}	Propene, trans-2-butene, cis-2-butene, 2-Methyl-2-butene, *trans*-2-pentene, *cis*-2-pentene
3	E-$(CH_3)CHOO$	53	2.3×10^{-14} (**1.2×10^{4}**)	2.7×10^{-11} (**1.4×10^{4}**)	1.4×10^{-10}	Propene, trans-2-butene, cis-2-butene, 2-Methyl-2-butene, *trans*-2-pentene, *cis*-2-pentene
4	Z-$(CH_2R_a)CHOO$	**205**	1.5×10^{-18} (1)	4.3×10^{-15} (2)	2.7×10^{-11}	1-butene, *trans*-2-pentene, *cis*-2-pentene, 1-pentene, 1-hexene, limonene
5	E-$(CH_2R_a)CHOO$	74	1.6×10^{-14} (**8×10^{3}**)	1.7×10^{-11} (**8.5×10^{3}**)	1.4×10^{-10}	1-butene, *trans*-2-pentene, *cis*-2-pentene, 1-pentene, 1-hexene, limonene, γ-terpinene
6	Z-$(CH_2R_a)(CH_3)COO$	**689**	1.5×10^{-17} (8)	3.2×10^{-14} (16)	1.6×10^{-10}	2-methyl-1-butene, limonene, α-terpinene
7	E-$(CH_2R_a)\ (CH_3)COO$	**433**	9.0×10^{-18} (5)	2.1×10^{-14} (11)	1.6×10^{-10}	2-methyl-1-butene, limonene, γ-terpinene, α-terpinene
8	$(CH_3)_2COO$	**478**	7.5×10^{-18} (4)	1.8×10^{-14} (9)	1.6×10^{-10}	2-methyl-2-butene
9	Z-MVK-oxide	**1.3×10^{4}** *2140* [a) c)]	1.8×10^{-18} (1)	4.8×10^{-15} (2)	1.6×10^{-10}	isoprene
10	E-MVK-oxide	**33** [a) b)] 70 [d)]	8.1×10^{-20} (0.04)	3.1×10^{-16} (0.2)	4.2×10^{-11} [b)]	isoprene
11	Z-MACR- oxide	**1.4×10^{4}**	1.2×10^{-19} (0.1)	4.3×10^{-16} (0.2)	1.6×10^{-10}	isoprene
12	E-MACR- oxide	**30**	1.4×10^{-16} (**70**)	2.7×10^{-13} (**135**)	1.6×10^{-10}	isoprene
13	Z-pinonaldehyde-K- oxide	**60**	2.4×10^{-19} (0.1)	8.9×10^{-16} (0.4)	1.6×10^{-10}	α-pinene
14	E-pinonaldehyde-K- oxide	**250**	9.8×10^{-18} (5)	3.2×10^{-15} (2)	1.6×10^{-10}	α-pinene
15	Z-pinonaldehyde-A-oxide	**634**	1.3×10^{-18} (1)	3.6×10^{-15} (2)	2.7×10^{-11}	α-pinene
16	E-pinonaldehyde-A-oxide	62	1.6×10^{-14} (**8×10^{3}**)	1.7×10^{-11} (**8.5×10^{3}**)	1.4×10^{-10}	α-pinene
17	Z-Nopinone oxide	2	4.2×10^{-16} (**210**)	6.0×10^{-13} (**300**)	4.0×10^{-11}	β-pinene
18	E-Nopinone oxide	**375**	1.7×10^{-18} (1)	3.7×10^{-15} (2)	1.6×10^{-10}	β-pinene
19	Z-(CRaRbRc)(CHRdRe)COO	1.1	2.4×10^{-17} (**12**)	4.5×10^{-14} (**23**)	1.6×10^{-10}	Camphene
20	E-(CRaRbRc)(CHRdRe)COO	1	3.2×10^{-17} (**16**)	5.9×10^{-14} (**30**)	1.6×10^{-10}	Camphene
21	Z-$(CHR_aR_b)(CH_3)COO$	**14**	9.8×10^{-18} (**5**)	1.9×10^{-14} (**10**)	1.6×10^{-10}	Limonene
22	E-$(CHR_aR_b)(CH_3)COO$	**611**	4.3×10^{-18} (2)	1.1×10^{-14} (6)	1.6×10^{-10}	Limonene
23	Z-$(CH_2\text{-}CR_3{=}CR_4R_5)CHOO$	**4180**	1.5×10^{-18} (1)	3.9×10^{-15} (2)	2.7×10^{-11}	γ-terpinene
24	Z-$(CH_2\text{-}CR_3{=}CR_4R_5)(CH_3)COO$	**1400**	4.1×10^{-18} (2)	2.9×10^{-14} (15)	1.6×10^{-10}	γ-terpinene
25	Z-$(CH_2\text{-}CR_3{=}CR_4R_5)(CHR_aR_b)COO$	**5250**	3.4×10^{-17} (17)	6.1×10^{-14} (31)	1.6×10^{-10}	γ-terpinene
26	Z-$(CHR_aR_b)(CH_2R_a)COO$	**13**	1.3×10^{-17} (**7**)	2.8×10^{-14} (**14**)	1.6×10^{-10}	γ-terpinene, α-terpinene
27	E-$(CH_2R_a)(CHR_aR_b)COO$	**257**	3.5×10^{-17} (18)	6.8×10^{-14} (34)	1.6×10^{-10}	α-terpinene
28	Z-$(CR_3{=}CR_4CH_3)CHOO$	**4.8×10^{6}**	1.2×10^{-19} (0.1)	4.3×10^{-16} (0.2)	2.7×10^{-11}	α-terpinene
29	E-$(CR_3{=}CR_4CH_3)CHOO$	30	1.4×10^{-16}	2.7×10^{-13}	1.4×10^{-10}	α-terpinene

			(**70**)	(**135**)		
30	Z-(C(O)R_a)CHOO	20	3.7×10^{-15} (**1850**)	4.4×10^{-12} (**2200**)	2.7×10^{-11}	MVK, EVK
31	E-(C(O)R_3)CHOO	0.04	5.1×10^{-18} (**3**)	1.4×10^{-14} (**7**)	1.4×10^{-10}	MVK, EVK, Acrolein
32	Z-(C(O)H)(CH_3)COO	**7.1×10^{4}**	1.4×10^{-14} (7×10^{3})	1.5×10^{-11} (7.5×10^{3})	1.6×10^{-10}	MACR
33	E-(C(O)R_3)(CH_3)COO	**3.8**	9.8×10^{-21} (0.005)	4.4×10^{-17} (0.02)	1.6×10^{-10}	MACR
34	Z-(C(O)H)CHOO	144	7.7×10^{-16} (**385**)	1.1×10^{-12} (**550**)	2.7×10^{-11}	Acrolein
35	Z-($CR_aR_bR_c$)CHOO	0.01	1.0×10^{-18} (**1**)	2.8×10^{-15} (**1**)	2.7×10^{-11}	Styrene
36	E-($CR_aR_bR_c$)CHOO	111	4.5×10^{-14} (**2.3×10^{4}**)	4.7×10^{-11} (**2.3×10^{4}**)	1.4×10^{-10}	Styrene

*) SCIs naming convention and rate coefficients are from (Vereecken et al., 2017) recommendations based on available measurements or theoretically derived SARs, except when otherwise noted.
A) In bold are presented the major loss pathways.
B) In parenthesis are presented the corresponding loss rate in s^{-1} at median during [H_2O] and [$(H_2O)_2$] ChArMEx.
a) (Barber et al., 2018)
b) (Caravan et al., 2020)
c) Experimental results of (Caravan et al., 2020) suggest faster unimolecular decay of Z-MVK-oxide in better agreement with results of (Vereecken et al., 2017)
d) (Lin et al., 2020)

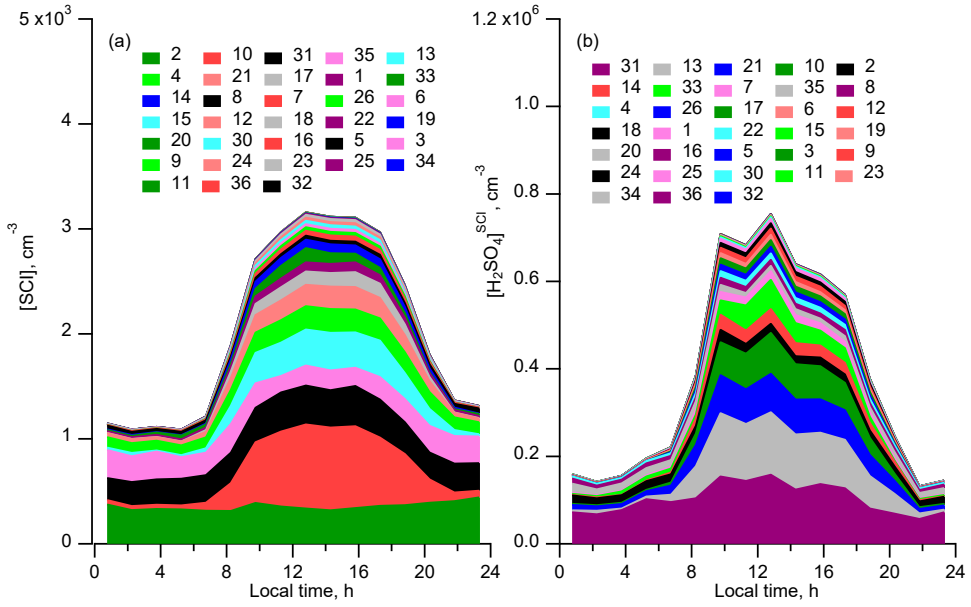

Figure S10. Calculated median diel concentration profiles of SCIs (a) produced by ozonolysis of measured unsaturated VOCs and of $H_2SO_4^{SCI}$ (b) produced by these SCIs in reaction with SO_2. The numbers correspond to the SCIs listed in Tables S4 and S5.

S5 Validity of H_2SO_4 steady state approximation

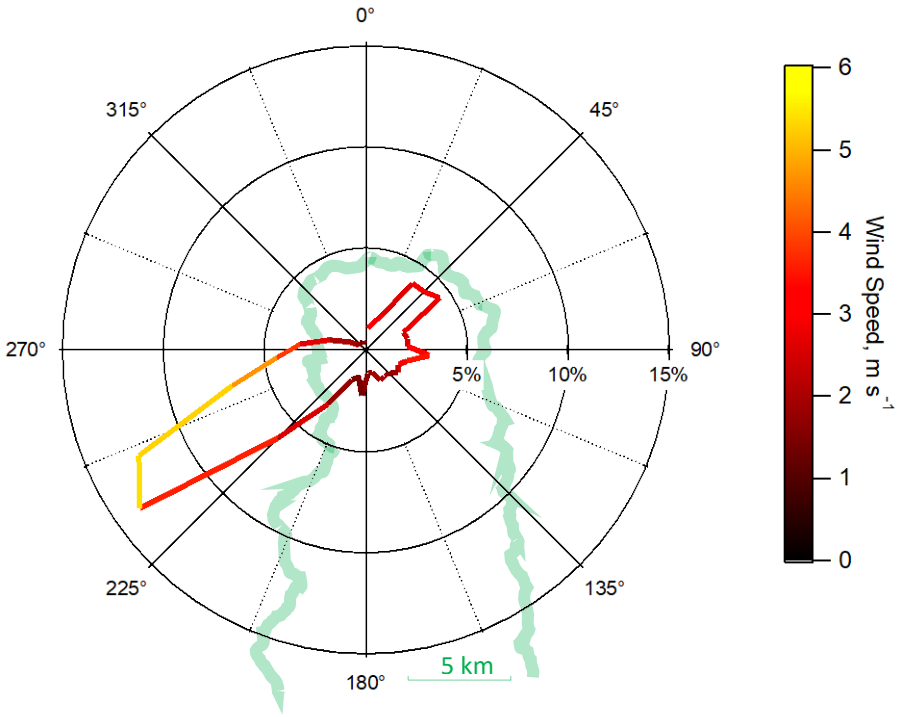

Figure S11. Wind direction probability centered at the Ersa measurements site and color coded median wind speed. Green curve represents the Cap Corse coastline

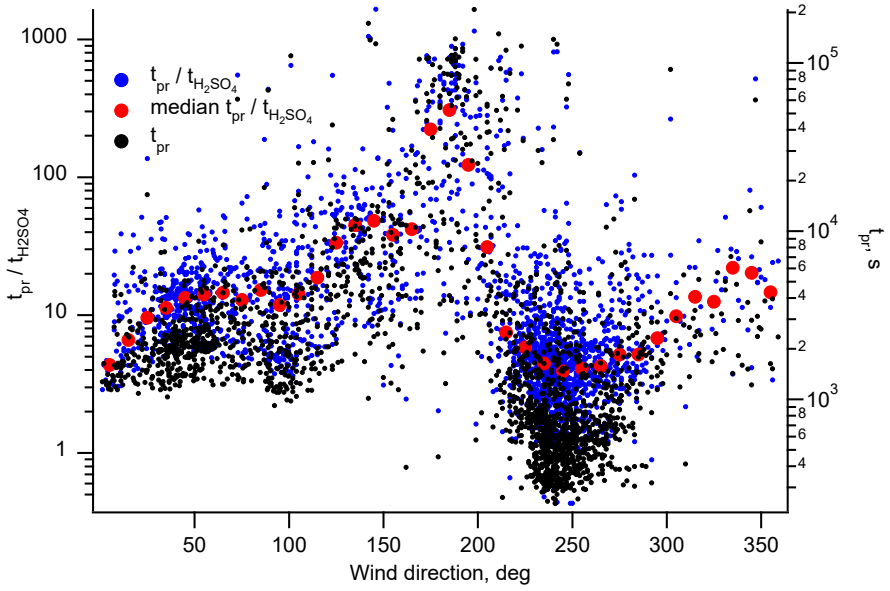

Figure S12. Ratio of air mass presence time over the land to H_2SO_4 lifetime, t_{pr} / t_{H2SO4}, (blue points) and the presence time t_{pr} (black points) as functions of the wind direction. Red points – median values of the ratios of t_{pr} / t_{H2SO4}.

S6 Importance of nucleation as a loss pathway of H_2SO_4

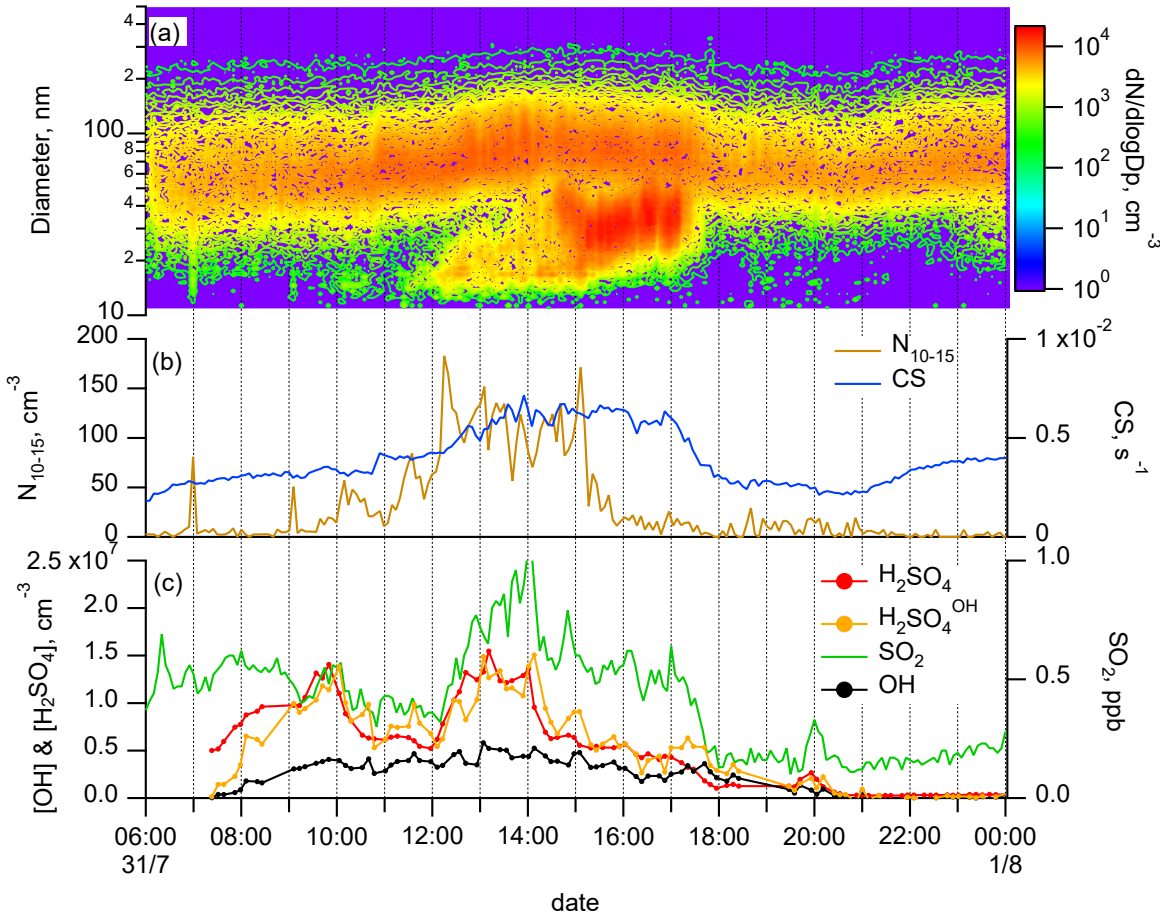

Figure S13. Example of new particles formation event (NPF) observed on 31 of July at Ersa station. (a) Time evolution of particle size distribution measured with SMPS. (b) Time profiles of the condensation sink (CS) and of the number concentration of 10–15 nm particles ($N_{10\text{-}15}$). (c) Concentration time profiles of measured OH radicals, H_2SO_4, SO_2 and calculated $H_2SO_4^{OH}$, the sulfuric acid produced via OH+SO_2.

S7 SCIs interference with OH and H_2SO_4 measurements

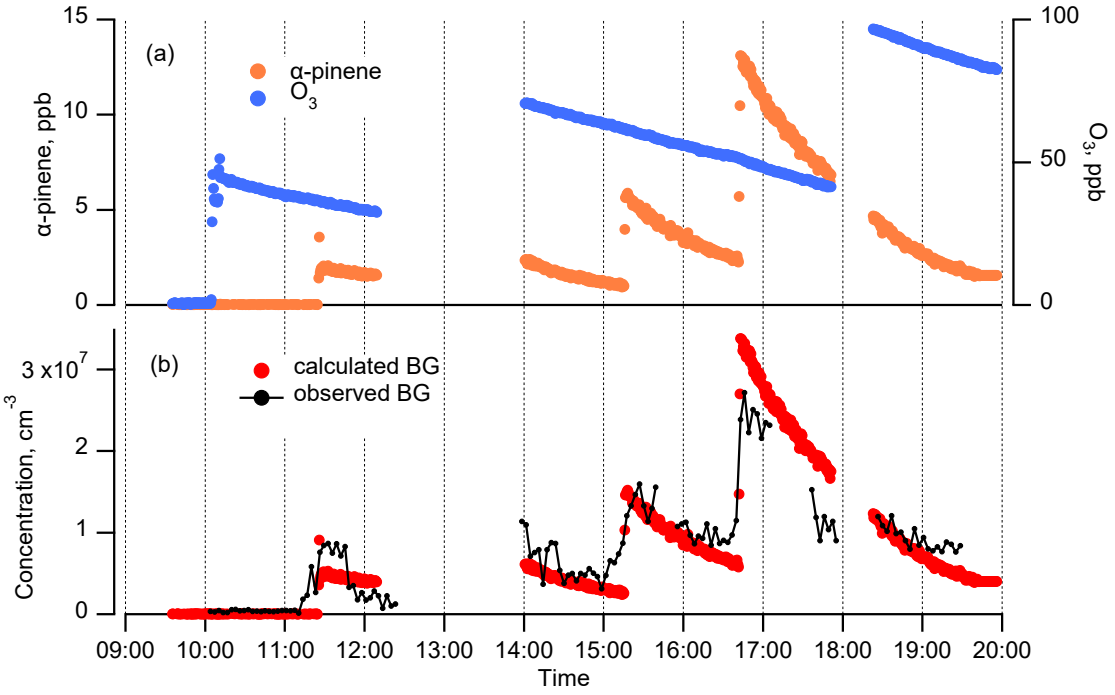

Figure S14. Example of a chamber study of the α-pinene ozonolysis showing dependence of background level (BG) on the SCI production rate: (a) α-pinene and ozone concentrations, (b) observed (black) and calculated (red) background levels. The calculations were made assuming O_3 concentration of 2 ppm in the IMR.

References

Atkinson, R., Baulch, D. L., Cox, R. A., Crowley, J. N., Hampson, R. F., Hynes, R. G., Jenkin, M. E., Rossi, M. J. and Troe, J.: Evaluated kinetic and photochemical data for atmospheric chemistry: Volume I - gas phase reactions of O_x, HO_x, NO_x and SO_x species, Atmos. Chem. Phys., 4(6), 1461–1738, doi:10.5194/acp-4-1461-2004, 2004.

Atkinson, R., Baulch, D. L., Cox, R. A., Crowley, J. N., Hampson, R. F., Hynes, R. G., Jenkin, M. E., Rossi, M. J., Troe, J. and IUPAC Subcommittee: Evaluated kinetic and photochemical data for atmospheric chemistry: Volume II – gas phase reactions of organic species, Atmos. Chem. Phys., 6(11), 3625–4055, doi:10.5194/acp-6-3625-2006, 2006.

Avzianova, E. V. and Ariya, P. A.: Temperature-dependent kinetic study for ozonolysis of selected tropospheric alkenes, Int. J. Chem. Kinet., 34(12), 678–684, doi:10.1002/kin.10093, 2002.

Barber, V. P., Pandit, S., Green, A. M., Trongsiriwat, N., Walsh, P. J., Klippenstein, S. J. and Lester, M. I.: Four-Carbon Criegee Intermediate from Isoprene Ozonolysis: Methyl Vinyl Ketone Oxide Synthesis, Infrared Spectrum, and OH Production, J. Am. Chem. Soc., 140(34), 10866–10880, doi:10.1021/jacs.8b06010, 2018.

Bardouki, H., Berresheim, H., Vrekoussis, M., Sciare, J., Kouvarakis, G., Oikonomou, K., Schneider, J. and Mihalopoulos, N.: Gaseous (DMS , MSA , SO_2, H_2SO_4 and DMSO) and particulate (sulfate and methanesulfonate) sulfur species over the northeastern coast of Crete, Atmos. Chem. Phys., 3, 1871–1886, doi:10.5194/acp-3-1871-2003, 2003.

Berresheim, H., Elste, T., Tremmel, H. G., Allen, A. G., Hansson, H., Rosman, K., Maso, M. D., Mäkelä, J. M., Kulmala, M. and O'Dowd, C. D.: Gas-aerosol relationships of H_2SO_4, MSA , and OH : Observations in the coastal marine boundary layer at Mace Head , Ireland, J. Geophys. Res., 107, 1–12, doi:10.1029/2000JD000229, 2002.

Berresheim, H., Adam, M., Monahan, C., O'Dowd, C., Plane, J. M. C., Bohn, B. and Rohrer, F.: Missing SO_2 oxidant in the coastal atmosphere? - Observations from high-resolution measurements of OH and atmospheric sulfur compounds, Atmos. Chem. Phys., 14(22), 12209–12223, doi:10.5194/acp-14-12209-2014, 2014.

Birmili, W., Wiedensohler, A., Plass-Dülmer, C. and Berresheim, H.: Evolution of Newly Formed Aerosol Particles in the Continental Boundary Layer : A Case Study Including OH and H_2SO_4 Measurements, Geophys. Res. Lett., 27(15), 2205–2208, 2000.

Black, G., Sharpless, R. L. and Slanger, T. G.: Rate coefficients at 298 K for SO reactions with O_2, O_3, and NO_2, Chem. Phys. Lett., 90(1), 55–58, 1982.

Boy, M., Mogensen, D., Smolander, S., Zhou, L., Nieminen, T., Paasonen, P., Plass-Dülmer, C., Sipilä, M., Petäjä, T., Mauldin, L., Berresheim, H. and Kulmala, M.: Oxidation of SO_2 by stabilized Criegee intermediate (sCI) radicals as a crucial source for atmospheric sulfuric acid concentrations, Atmos. Chem. Phys., 13(7), 3865–3879, doi:10.5194/acp-13-3865-2013, 2013.

Burkholder, J. B., Sander, S. P., Abbat, J., Barker, J. R., Huie, R. E., Kolb, C. E., Kurylo, M. J., Orkin, V. L., Wilmouth, D. M. and Wine, P. H.: Chemical Kinetics and Photochemical Data for Use in Atmospheric Studies, Evaluation No. 18, JPL Publication 15-10, Jet Propulsion Laboratory, Pasadena, [online] Available from: http://jpldataeval.jpl.nasa.gov/, 2015.

Caravan, R. L., Vansco, M. F., Au, K., Khan, M. A. H., Li, Y.-L., Winiberg, F. A. F., Zuraski, K., Lin, Y.-H., Chao, W., Trongsiriwat, N., Walsh, P. J., Osborn, D. L., Percival, C. J., Lin, J. J.-M., Shallcross, D. E., Sheps, L., Klippenstein, S. J., Taatjes, C. A. and Lester, M. I.: Direct kinetic measurements and theoretical predictions of an isoprene-derived Criegee intermediate, Proc. Natl. Acad. Sci., 117(18), 9733–9740, doi:10.1073/pnas.1916711117, 2020.

Creasey, D. J., Heard, D. E. and Lee, J. D.: Absorption cross-section measurements of water vapour and oxygen at 185 nm . Implications for the calibration of field instruments to measure OH , HO_2 and RO_2 radicals, , 27(11), 1651–1654, 2000.

Danielache, S. O., Eskebjerg, C., Johnson, M. S., Ueno, Y. and Yoshida, N.: High-precision spectroscopy of ^{32}S , ^{33}S , and ^{34}S sulfur dioxide : Ultraviolet absorption cross sections and isotope effects, J. Geophys. Res. Atmos., 113, D17314, doi:10.1029/2007JD009695, 2008.

Dusanter, S., Vimal, D. and Stevens, P. S.: Technical note : Measuring tropospheric OH and HO_2 by laser-

induced fluorescence at low pressure . A comparison of calibration techniques, Atmos. Chem. Phys., 8, 321–340, 2008.

Eisele, F. L. and Tanner, D. J.: Measurement of the gas phase concentration of H_2SO_4 and methane sulfonic acid and estimetes of H_2SO_4 production and loss in the atmosphere, J. Geophys. Res., 98, 9001–9010, 1993.

Grosjean, E., Grosjean, D. and Williams, E. L.: Rate constants for the gas-phase reactions of Ozone with unsaturated Alcohols, Esters and Carbonyls, Int. J. Chem. Kinet., 25, 783, doi:10.1002/kin.550261206, 1993.

IUPAC: Task Group on Atmospheric Chemical Kinetic Data Evaluation, http://iupac.pole-ether.fr, last access: April, 2020.

Jefferson, A., Tanner, D. J., Eisele, F. L. and Berresheim, H.: Sources and sinks of H_2SO_4 in the remote Antarctic marine boundary layer, J. Geophys. Res. Atmos., 103(D1), 1639–1645, doi:10.1029/97JD01212, 1998.

Kim, S., Guenther, A., Lefer, B., Flynn, J., Griffin, R., Rutter, A. P., Gong, L. and Cevik, B. K.: Potential role of stabilized Criegee radicals in sulfuric acid production in a high biogenic VOC environment, Environ. Sci. Technol., 49(6), 3383–3391, doi:10.1021/es505793t, 2015.

Kürten, A., Rondo, L., Ehrhart, S. and Curtius, J.: Calibration of a Chemical Ionization Mass Spectrometer for the Measurement of Gaseous Sulfuric Acid, J. Phys. Chem. A, 116, 6375–6386, 2012.

Lin, Y.-H., Yang, C., Takahashi, K. and Lin, J. J.-M.: Kinetics of Unimolecular Decay of Methyl Vinyl Ketone Oxide, an Isoprene-Derived Criegee Intermediate, under Atmospherically Relevant Conditions, J. Phys. Chem. A, 124, 9375–9381, doi:10.1021/acs.jpca.0c07928, 2020.

Mauldin III, R. L., Berndt, T., Sipilä, M., Paasonen, P., Petäjä, T., Kim, S., Kurtén, T., Stratmann, F., Kerminen, V.-M. and Kulmala, M.: A new atmospherically relevant oxidant of sulphur dioxide, Nature, 488(7410), 193–196, doi:10.1038/nature11278, 2012.

Novelli, A., Vereecken, L., Lelieveld, J. and Harder, H.: Direct observation of OH formation from stabilised Criegee intermediates, Phys. Chem. Chem. Phys., 16(37), 19941–19951, doi:10.1039/C4CP02719A, 2014.

Novelli, A., Hens, K., Ernest, C. T., Martinez, M., Nölscher, A. C., Sinha, V., Paasonen, P., Petäjä, T., Sipilä, M., Elste, T., Plass-Dülmer, C., Phillips, G. J., Kubistin, D., Williams, J., Vereecken, L., Lelieveld, J. and Harder, H.: Estimating the atmospheric concentration of Criegee intermediates and their possible interference in a FAGE-LIF instrument, Atmos. Chem. Phys., 17(12), 7807–7826, doi:10.5194/acp-17-7807-2017, 2017.

Le Person, A., Eyglunent, G., Daële, V., Mellouki, A. and Mu, Y.: The near UV absorption cross-sections and the rate coefficients for the ozonolysis of a series of styrene-like compounds, J. Photochem. Photobiol. A Chem., 195(1), 54–63, doi:10.1016/j.jphotochem.2007.09.006, 2008.

Petäjä, T., Mauldin III, R. L., Kosciuch, E., McGrath, J., Nieminen, T., Paasonen, P., Boy, M., Adamov, A., Kotiaho, T. and Kulmala, M.: Sulfuric acid and OH concentrations in a boreal forest site, Atmos. Chem. Phys., 9, 7435–7448, 2009.

Sander, S. P., Abbatt, J., Barker, J. R., Burkholder, J. B., Friedl, R. R., Golden, D. M., Huie, R. E., Kolb, C. E., Kurylo, M. J., Moortgat, G. K., Orkin, V. L. and Wine, P. H.: Chemical Kinetics and Photochemical Data for Use in Atmospheric Studies, Evaluation No. 17," JPL Publication 10-6, Jet Propulsion Laboratory, Pasadena, http://jpldataeval.jpl.nasa.gov, 2011.

Tennekes, H. and Lumley, J. L.: A first course in turbulence, Cambridge, Mass. : MIT Press., 1972.

Vereecken, L., Novelli, A. and Taraborrelli, D.: Unimolecular decay strongly limits the atmospheric impact of Criegee intermediates, Phys. Chem. Chem. Phys., 19, 31599–31612, doi:10.1039/C7CP05541B, 2017.

Weber, R. J., Marti, J. J., Mcmurry, P. H., Eisele, F. L., Tanner, D. J. and Jefferson, A.: Measurements of new particle formation and ultrafine particle growth rates at a clean continental site, J. Geophys. Res., 102, 4375–4385, 1997.

Whitehill, A. R., Jiang, B., Guo, H. and Ono, S.: SO_2 photolysis as a source for sulfur mass-independent isotope signatures in stratospehric aerosols, Atmos. Chem. Phys., 15, 1843–1864, doi:10.5194/acp-15-1843-2015, 2015.

Witter, M., Berndt, T., Böge, O., Stratmann, F. and Heintzenberg, J.: Gas-phase ozonolysis: Rate coefficients for a series of terpenes and rate coefficients and OH yields for 2-methyl 2-butene and 2,3-dimethyl-2-butene, Int. J. Chem. Kinet., 34(6), 394–403, doi:10.1002/kin.10063, 2002.

Zhang, D., Lei, W. and Zhang, R.: Mechanism of OH formation from ozonolysis of isoprene: Kinetics and product yields, Chem. Phys. Lett., 358(3–4), 171–179, doi:10.1016/S0009-2614(02)00260-9, 2002.